Applied Catalysis B: Environmental 214 (2017) 158–167

Contents lists available at ScienceDirect

Applied Catalysis B: Environmental

journal homepage: www.elsevier.com/locate/apcatb

Synthesis of MFe_2O_4 (M = Ni, Co)/$BiVO_4$ film for photoelectrochemical hydrogen production activity

Qizhao Wang[a,*], Jijuan He[a], Yanbiao Shi[a], Shuling Zhang[a], Tengjiao Niu[a], Houde She[a], Yingpu Bi[b,*], Ziqiang Lei[a]

[a] College of Chemistry and Chemical Engineering, Northwest Normal University, Key Laboratory of Eco-Environment-Related Polymer Materials, Ministry of Education of China, Lanzhou 730070, China
[b] State Key Laboratory of Oxo Synthesis & Selective Oxidation, National Engineering Research Central for Fine Petrochemical Intermediates Lanzhou Institute of Chemical Physics, CAS, Lanzhou 730000, China

ARTICLE INFO

Article history:
Received 9 February 2017
Received in revised form 25 April 2017
Accepted 16 May 2017
Available online 18 May 2017

Keywords:
Fruticose dracaena leaf-like structure
$MFe_2O_4/BiVO_4$ (M = Ni
Co) composite
PEC performance
Hydrogen production

ABSTRACT

The leaf-like structure $BiVO_4$ electrode and $MFe_2O_4/BiVO_4$ (M = Ni, Co) composite photoelectrodes were prepared by electrochemical deposition, ensuing heating treatment and electrophoretic deposition technology. The characterizations of SEM, XRD and DRS indicated that the $BiVO_4$ derivatives mainly existed in small nanoparticles with monoclinic phase and exhibited stronger light absorption capability than that of pure $BiVO_4$. Hereon, the respective photoelectrochemical (PEC) activities of $BiVO_4$ and its derived composites were systematically studied. The results suggested that the $NiFe_2O_4/BiVO_4$ and $CoFe_2O_4/BiVO_4$ not only showed higher photocurrent response values at 1.23 V vs. NHE than pure $BiVO_4$ electrode under visible light illumination, but also played a superior PEC hydrogen evolution performance, which was considered owing to their strong absorption to light, reduction combination of carriers and effective separation of electrons and holes.

1. Introduction

Hydrogen, a clean and renewable energy, has been increasingly drawed extensive interests due to the growing resource shortage and environmental pollution. Since the first report regarding TiO_2 photoanode in 1972, PEC cell employing a huge varity of semiconductor-based materials as photoanode are much more intensively studied due to its outstanding efficiency in hydrgen generation, such as TiO_2, WO_3 and Fe_2O_3 [1–3]. Among these well-applied materials, $BiVO_4$, a narrow-energy-gap (Eg = 2.4–2.5 eV) n-type semiconductor,exhibits excellent capacities of absorption to visible light, adjustable electronics structure, good stability and low cost of preparation [4–6]. Although the conduction band position of $BiVO_4$ is close to 0 V vs. NHE that is less than water reduction potential and thus make it difficult to directly produce hydrogen under visible light illumination. In this case, a bais is generally required to accelerate the reaction process [7,8]. Besides, using $BiVO_4$ photoanode alone cannot generate acceptable photocurrent at lower potential due to the rapid combination of electron-hole pairs during the reduction process, which results in a much lower actual photocurrent value than that caculated theoretically (~7 mA cm^{-2} under AM 1.5G) [9].

In order to overcome these limitations and make full use of solar energy to gain hydrogen energy, morphology tuning and surface modification for the materials have been primarily attempted to improve the PEC performance of $BiVO_4$ photoanode [10–12]. Dip-coating, metal-organic decomposition, straightly pasting or spin-coating [13–15], all these simple menthods are able to yield $BiVO_4$ in thin film. However, the as-prepared films were relatively thick and heterogeneous. In fact, both thickness and uniformity of the materials would influence their capacities in a large extent. Using reactive ballistic deposition (RBD) and pulsed laser deposition (PLD) technology, respectively [16,17], either the successfully prepared nanostructure $BiVO_4$ film and the $BiVO_4/WO_3/SnO_2$ ternary displayed great charge transport property. Based on the electrochemical deposition procedure, nanoporous $BiVO_4$ electrodes showing excellent PEC performance were further obtained via electrochemically depositing BiOI electrode by Tae Woo Kim and Kyoung-Shin Choi [10]. Before many other studies focusing on the surface modification by co-catalysts for oxygen production and heterojunctions formation via combining other semiconductors to improve the PEC activity of nanoporous $BiVO_4$ [18,19]. There are other methods that have been scrupulously designed to pre-

* Corresponding authors.
E-mail addresses: wangqizhao@163.com, qizhaosjtu@gmail.com (Q. Wang), yingpubi@licp.cas.cn (Y. Bi).

http://dx.doi.org/10.1016/j.apcatb.2017.05.044
0926-3373/

pare $BiVO_4$ films [20,21]. Xiang's group synthesized dendrite-free bismuth via exploiting self-healing electrostatic shield mechanism [22], in which Zn^{2+} ions were introduced as a direct agent to control the morphology and size of Bi nanoparticles [23].

The construction of heterojunction with other semiconductor is also an efficient approach to improve catalytic activity. Recently, photo-electrodes based on $BiVO_4$ composites, like $BiOI/BiVO_4$, $WO_3/BiVO_4$, $CaFe_2O_4/BiVO_4$, $ZnO/BiVO_4$ and $TiO_2/BiVO_4$ heterojunction photoanodes have been broadly investigated [24–26]. The magnetic semiconductors $NiFe_2O_4$ and $CoFe_2O_4$ are typical n-type and p-type semiconductors both possessing strong absorption capacity under UV and visible light irradiation and hence widely used for photocatalytic reaction, such as the application of $CoFe_2O_4/BiVO_4$ powder in decomposing dye molecules [27–30]. Whereas, the PEC performances of the heterojunction construction combined by $BiVO_4$ and magnetic semiconductors are rarely reported as far as we know.

In this work, Zn^{2+} ions were added as structure-directing agent. When the concentration of Bi $(NO_3)_3$ electrolyte was increased, the morphology of Bi metallic particle would change correspondingly. A fruticose dracaena like-leaf Bi precursor film was obtained in the electrolyte at a high concentration. The final $BiVO_4$ film still sustained the same morphology as the initial Bi film, which differed from the published literature [23]. Zn^{2+} ions also played the role of rapidly depositing bismuth metal, resulting in a fascinating $BiVO_4$ structure. $NiFe_2O_4$ and $CoFe_2O_4$ nanoparticles were further decorated on the surface of $BiVO_4$ film by electrophoretic deposition, capacitating the binary compounds exhibiting excellent PEC activities.

2. Experimental

2.1. Materials and characterization

$Bi(NO_3)_3{\cdot}5H_2O$ (Sinopharm Chemical Reagent Co., Ltd, 99.0%), $Ni(NO_3)_3{\cdot}6H_2O$ (Sinopharm Chemical Reagent Co., Ltd, 98.5%), $Co(CH_3COO)_2{\cdot}4H_2O$ (Sinopharm Chemical Reagent Co., Ltd, 99%), $Zn(NO_3)_3{\cdot}6H_2O$ (Aladdin, 99%), Fe_2O_3 (Tianjin kaixin chemical industry co., LTD, 69.8%-70.1%).

The X-ray diffraction pattern of all the electrodes were recorded on a Rigaku X-ray diffractometer D/Max-2200/PC equipped with Cu-Ka radiation (40kv, 20 mA). The optical properties of all samples were estimated by double-beam UV–vis spectrophotometer (PuXin TU-1901) equipped with an integrating sphere attachment using $BaSO_4$ as a reflectance sample. The structure and morphology of all films was observed from a JSM-6701E field emission scanning electron microscope (FE-SEM). TEM test was carried out on a TECNAI TF20 instrument. XPS analysis was recorded on PHI5702 photoelectron spectrometer. The photoluminescence (PL) spectra of films were measured at room temperature under 350 nm excitation wavelength (PE, LS-55).

2.2. Synthesis of fruticose dracaena leaf structure Bi precursor film and $BiVO_4$ photoelectrode, $NiFe_2O_4$ and $CoFe_2O_4$ powder, $NiFe_2O_4/BiVO_4$ and $CoFe_2O_4/BiVO_4$ films

Bi precursor films were prepared via learning from a facile electrochemical deposition technique [23]. This method was different from a general method, in which $Zn^{2+}$was added into the electrolyte as a directing agent instead of traditional hard template to tailor the structure and particle size of Bi precursor film. Therefore, we selected the as-reported optimal addition of Zn^{2+} (Zn/Bi = 3), and the whole electrolyte concentration was expanded to different multiples. A very inerratic fruticose dracaena leaf structure Bi precursor film was obtained in a short time at room temperature. Typically, the electrolyte was consisted of 100 mL ethylene glycol and 50 mL distilled water containing 0.01 mol $Bi(NO_3)_3{\cdot}5H_2O$, 0.03 mol $Zn(NO_3)_2{\cdot}6H_2O$. The 1*2.5 cm F-doped SnO_2 coated glass (FTO) conductive substance was used for the working electrode, the Ag/AgCl (3.5 M) and the wire slice were considered as reference electrode and counter electrode, respectively. The electro-deposition was performed by chronoamperomety (i-t) in −0.6 V constant potential at a 50 mV/ s of scan rate for 200s. After that, the resulting Bi films were completely washed with absolute ethanol and dried in ambient air. In order to reap $BiVO_4$ film, 0.1 mL 0.2 mol/L $VO(acac)_2$ DMSO solution was dropped onto the as-prepared Bi precursor films using syringe dispensing, and these films were sintered at 450 °C for 2 h in the air at a heating rate of 2 °C/min. After naturally cooling down the room temperature, the films were taken out immediately and immersed in 0.1 M NaOH solution to remove excess Bi_2O_3 and V_2O_5 impurity.

$NiFe_2O_4$ and $CoFe_2O_4$ were obtained by grinding calcinations method. Specifically, Ni $(NO_3)_2{\cdot}6H_2O$ and Co $(CH_3COO)_2{\cdot}4H_2O$ were regarded as nickel source and cobalt source, respectively. Then moderate Fe_2O_3 were mixed with the above nickel nitrate and cobalt acetate by grinding with addition of a little absolute ethanol in a mortar, respectively. After continuously reciprocating grinding for 30 min, the resulting two mixtures were encapsulated into porcelain to heat at 800 °C for 6 h. Finally, the rest of production was collected and grinded to powder.

The $NiFe_2O_4$ and $CoFe_2O_4$ nanoparticles were decorated successfully $BiVO_4$ electrode by a simple electrophoretic deposition. In details, 40 mg $NiFe_2O_4$ and $CoFe_2O_4$ powder were added into the 50 mL acetone solution including 10 mg I_2, respectively. These mixture solutions were dispersed by a vigorous sonication for 40 min. As-obtained leaf structure $BiVO_4$ electrodes were injected into the suspension and connected to the CD power negative pore, another new FTO glass was parallel to the $BiVO_4$ electrode and connected to the positive pore. Then, the electrophoretic deposition was performed on a CD powder (LW-3010DCX) at 20 V of bias for 10 s and 15 s, respectively. All of experimental process is simply presented Fig. 1.

2.3. Photoelectrochemical performance (PEC) and photoelectrochemical hydrogen evolution measurement

All of the photoelectrochemical performance measurements were carried out on a CHI 660D electrochemical workstation (CHI Shanghai) with typical three electrodes cell under the 350 W Xenon lamp (λ > 420 nm, CEL-S500) as light source illumination. Three electrodes were working electrode of photoanodes, Ag/AgCl as reference electrode and wire slice as assistance electrode, respectively. The electrolyte was 0.5 M Na_2SO_4 (pH~7.35) solution. All of the measurements were irradiated from the back side of working electrode with about 2 cm^{-2} areas. The scan rate in the current−voltage measurements was 25 mV s^{-1}, the bias of applied in the current-time test was 1.23 V vs. RHE, and the electrochemical impedance spectroscopy (EIS) was implemented at open circuit potential with a 0.01 V amplitude perturbation between 100 kHz and 0.1 Hz. The incident-photo-current conversion efficiency (IPCE) was assessed with a Xenon lamp (PLS-SXE300C) equipped with a monochromator (71SWS, Beijing 7-Star Optical Instruments Co., Ltd.) at 1.23 V vs. RHE bias in 0.2 M Na_2SO_4 solution. Mott−Schottky plots were recorded in 0.2 M Na_2SO_4 at a frequency of 1 kHz in the dark. All involved potential in this work has been converted to vs RHE according to following equation:

$$E_{vs.\ RHE} = E_{vs.\ Ag/AgCl} + E_{Ag/AgCl\ vs.\ NHE} + 0.059pH$$

$E_{Ag/AgCl\ vs.\ NHE}$ is 0.197 V at room temperature.

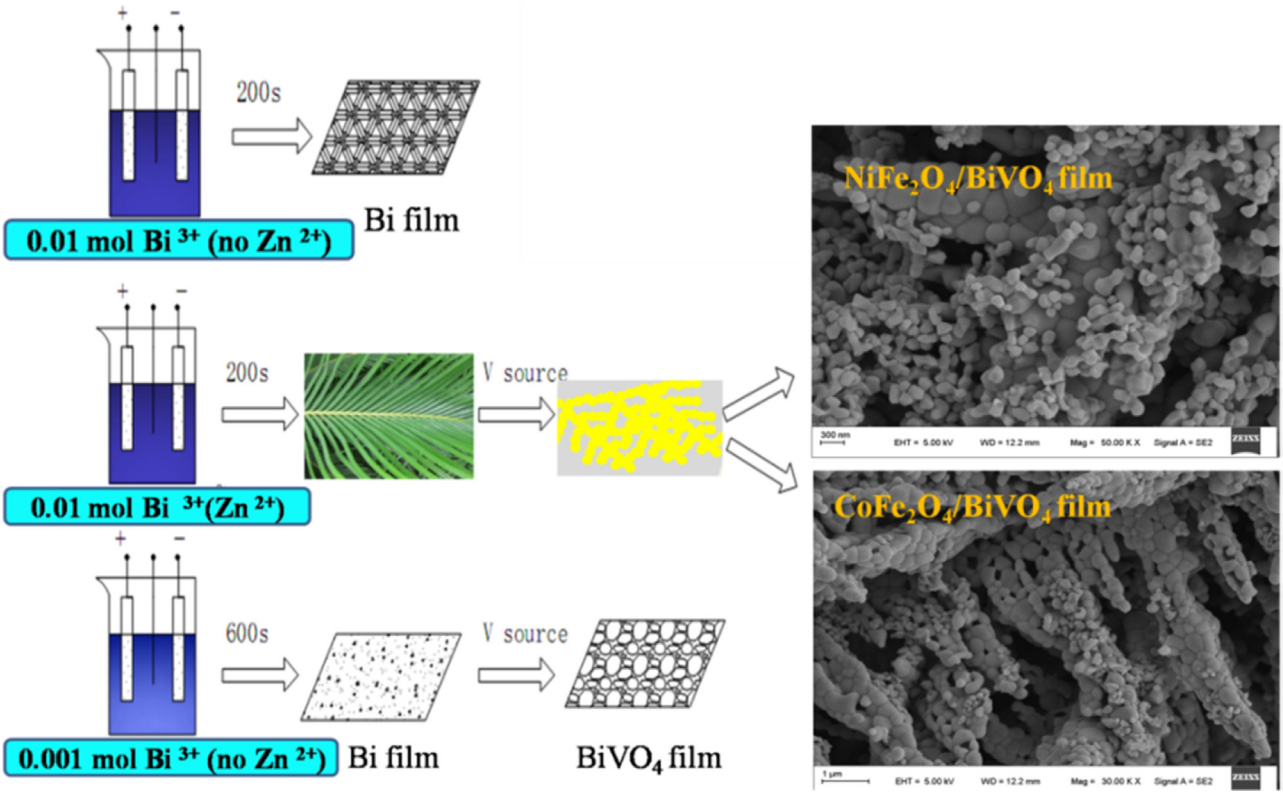

Fig 1. Synthesis schematic diagram of $BiVO_4$, $NiFe_2O_4/BiVO_4$ and $CoFe_2O_4/BiVO_4$ electrodes are from different concentration electrolytes and deposition time.

The hydrogen generation was valued by using a self-made H-type photo-reactor (Fig. S8). The 300 W Xenon lamp ($\lambda > 420$ nm, CEL-HXF300) was used as light source, 0.5 M Na_2SO_4 was considered as electrolyte and without adding any sacrificial agent. Argon was passed into the photo-reactor cell for 30 min before turning on the light to drive away the air in the reaction system. Produced hydrogen was collected with special extraction syringes and measured by gas chromatography (GC-9560).

3. Result and discussion

As reported in the previous work [23], the Bi film with small particle size and high density distribution was prepared on FTO glass substance after the addition of directing agent Zn^{2+} (Fig. S1). However, it can be found that the structure and morphology of Bi film presented obvious difference at various electrolyte concentration and amount of introduced Zn^{2+} ions. It is believed that the ions with more positive reduction potential might make it easier to reduce metal ions. According to the calculation of Nernst equation (Table S1), the increment of electrolyte concentration would enhance the reduction potential of Bi^{3+}/Bi, and thus it is conducive to rapid acquisition of metal film, which was further confirmed by the successfully prepared metallic Bi film with certain morphology via a relatively high electrolyte concentration within 200 s. Introducing Zn^{2+} ions to the Bi synthesis is evidently indispensable not only because the size of Bi metallic particles are controlled by Zn^{2+} ions in accordance with the self-healing electrostatic shield (SHES) mechanism, but also due to the rapid formation of regulate fruticose dracaena leaf-like structure (Fig. 2a). The measurement of PEC activities of all $BiVO_4$ derived from as-obtained Bi film at successive concentration of electrolytes for 200 s (Fig. S2). It indicated that the leaf-like structure Bi precursor film provides a foundation for the pattern of consequently synthesized $BiVO_4$ photoelectrode.

Fig. S1 and Fig. 1(a) displayed the profiles of $BiVO_4$ at different concentration of electrolytes. Surprisingly, the morphology of $BiVO_4$ film was almost the same as the fruticose dracaena leaf-like Bi film. The principal axis of leaves and the branched spikelet both were composed of Bi metallic nanoparticles. These particles mutually connected to regularly form side chains in the hollow leaves without observable aggregation. Leaf-like structure $BiVO_4$ at the diameter of 50–250 nm was determined by SEM, as shown in Fig. 2b. According to the published literature [31], the small nanoparticle is beneficial to the diffusion of holes. Meanwhile, the smooth surface and coverage in high density favors decreasing combination of carriers. In contrast, the rough surface might become a combination center for photo-induced electrons and holes [23]. A number of $NiFe_2O_4$ and $CoFe_2O_4$ small particles were dispersed evenly on the leaf-like structure $BiVO_4$ film after electrophoretic deposition, as shown in Fig. 2c and d. The investigated thickness of $BiVO_4$ film is around 5 μm (Fig. S3). Elemental mappings of $NiFe_2O_4/BiVO_4$ and $CoFe_2O_4/BiVO_4$ showed the presence of Bi, O, V, Ni, Co, Fe elements, indicating that the composite film has been successfully prepared (Fig. 3a and b).

The TEM and HRTEM images of sample were shown in Fig. 4. It was obvious that the $NiFe_2O_4$ and $CoFe_2O_4$ nanoparticles have been deposited on the surface of $BiVO_4$. The apparent lattice spacing of the synthesized samples was embodied in the HRTEM. The resolved interplanar distances were estimated to be about 0.473 and 0.309 nm, corresponding to the (110) plane of $BiVO_4$ and the (−121) plane of $BiVO_4$, respectively. The interplanar distance of 0.295 nm was consistent with $NiFe_2O_4$ (220) plane. For the $CoFe_2O_4/BiVO_4$ film, the interplanar distances were evaluated to be around 0.467 and 0.297 nm, attributing to the (011) plane of $BiVO_4$ and the (220) planar of $CoFe_2O_4$, respectively.

The crystalline phase structure and chemical composition of all photoelectrodes were measured by XRD pattern as shown in Fig. 5. All the diffraction peaks of $BiVO_4$ films were ascribed to mono-

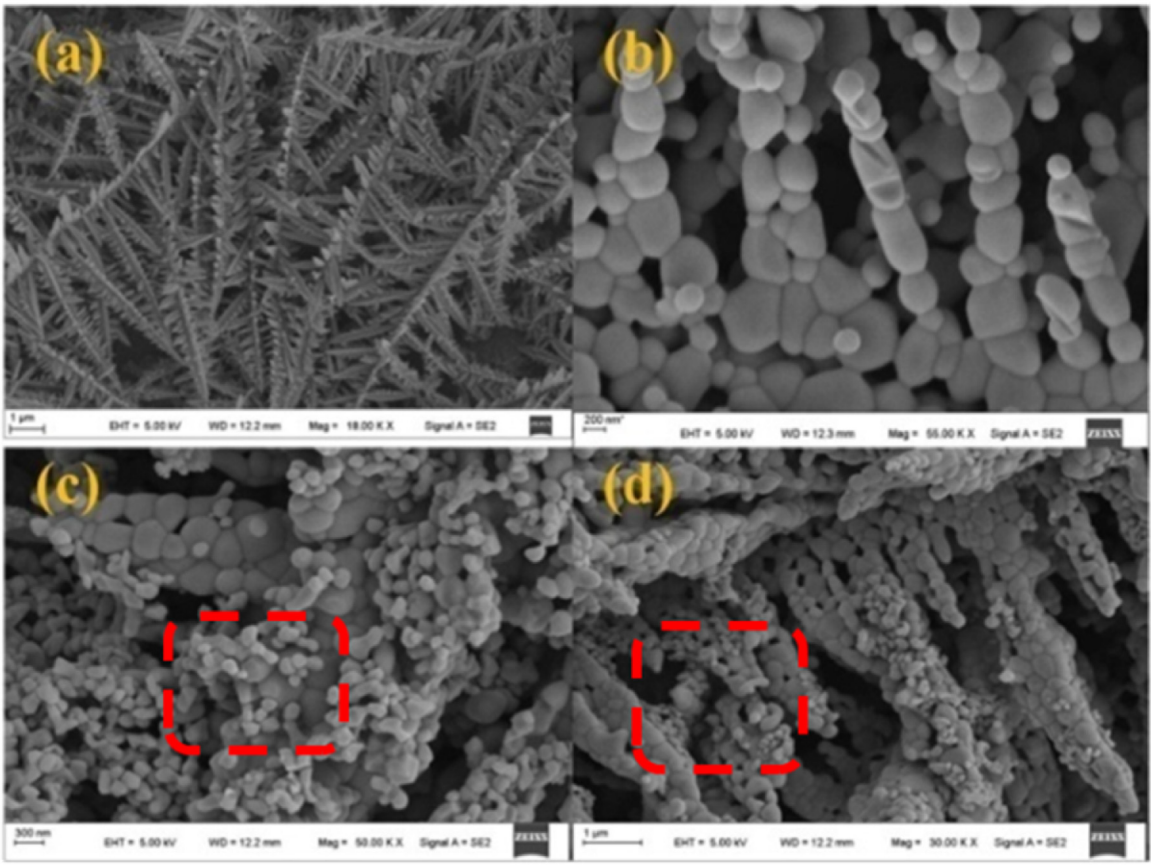

Fig. 2. The SEM images of (a) as-obtained Bi in high concentration electrolyte; (b) $BiVO_4$ from the fruticose dracaena leaf structure Bi precursor film; (c) $NiFe_2O_4/BiVO_4$ electrode; (d) $CoFe_2O_4/BiVO_4$ electrode.

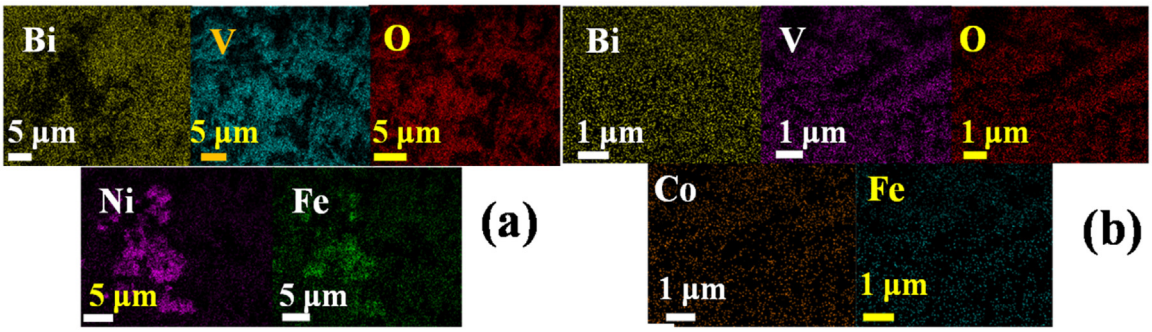

Fig. 3. Elemental mapping images of (a) $NiFe_2O_4/BiVO_4$ and (b) $CoFe_2O_4/BiVO_4$, respectively.

clinic crystal phase (PDF#14-0688), which might possess excellent photocatalysis activities as compared to the white tungsten-type square crystal phase and zircon-type square crystal phase [32,33]. No any impurity diffraction peaks can be observed for two pure $BiVO_4$ electrodes besides the peaks of SnO_2 (PDF#41-1445) of FTO substance (Fig. 4a and b). The peak intensity of $BiVO_4$ from regulate fruticose dracaena leaf-like structure Bi precursor film was stronger than that of the $BiVO_4$ from Bi nanoparticles film, indicating that its crystallinity degree is greater than the $BiVO_4$ film from Bi nanoparticles. After $BiVO_4$ film decorating with $NiFe_2O_4$ and $CoFe_2O_4$ nanoparticles, the main peak intensity of $BiVO_4$ electrode was not weakened, but the peak position slightly shifted, owing to their analogous diffraction peaks shifts at 18.8°, 30.8°, 36.0°, 54.4° [30]. Besides, no other apparent peaks of $NiFe_2O_4$ and $CoFe_2O_4$ were detected due to the less content [34]. In order to affirm the ingredient of $NiFe_2O_4$ and $CoFe_2O_4$ compounds, the XRD pattern and FTIR spectrum of $NiFe_2O_4$ and $CoFe_2O_4$ powder were shown in Fig. S4 and S5. According to the XRD pattern, a small amount of residual Fe_2O_3 was detected as well as the diffraction peaks of $NiFe_2O_4$ and $CoFe_2O_4$. In order to explore the influence of Fe_2O_3 on the PEC performance in $BiVO_4$ photoelectrode, the photocurrent and impedance of as-prepared $Fe_2O_3/BiVO_4$ in the same conditions were tested (Fig. S5). The results showed the photocurrent response of $Fe_2O_3/BiVO_4$ electrode was lower than $BiVO_4$, demonstrating that the photocurrent cannot be improved by the residual Fe_2O_3.

X-ray photoelectron spectroscopy (XPS) was employed to investigate the chemical compositions and oxidation states of samples. Fig. 6A showed the XPS spectra of Bi4f, V2p, O1s, Ni2p, Fe2p and C1s in the surface of $NiFe_2O_4/BiVO_4$. While Bi4f, V2p, O1s, Co2p,

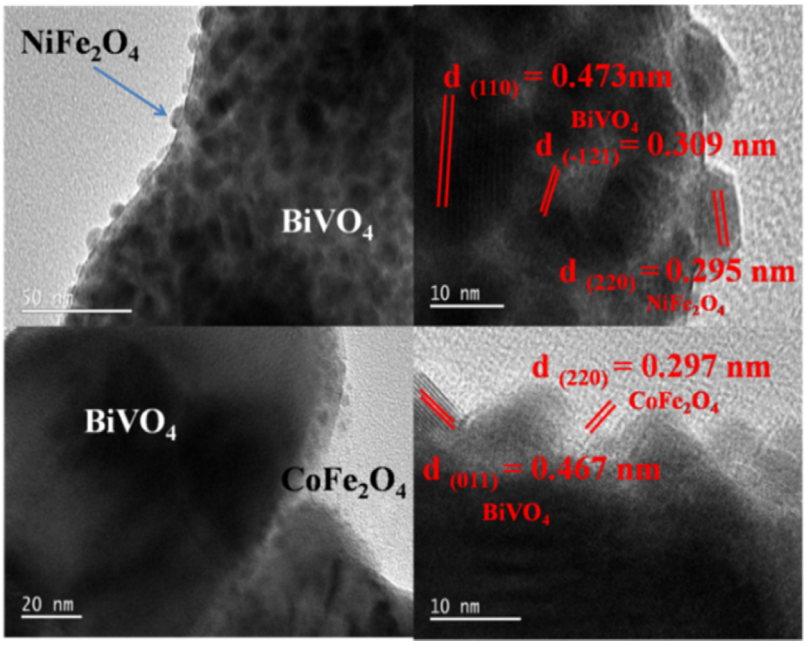

Fig. 4. TEM and HRTEM images of $NiFe_2O_4/BiVO_4$ and $CoFe_2O_4/BiVO_4$ films.

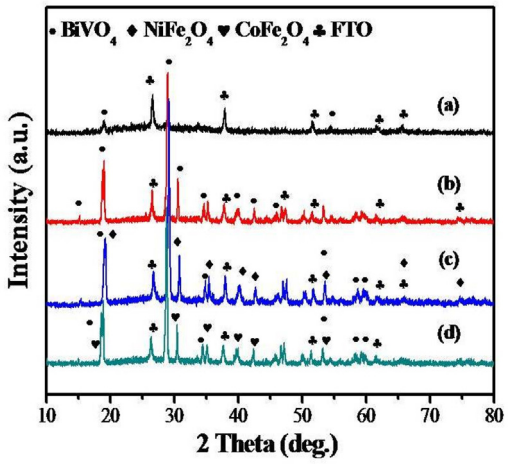

Fig. 5. XRD pattern of all electrodes (a) $BiVO_4$ is from Bi nanoparticles; (b) $BiVO_4$ comes from regulate fruticose dracaena leaf structure Bi precursor film; (c) $NiFe_2O_4/BiVO_4$ film; (d) $CoFe_2O_4/BiVO_4$ film.

Fe2p and C1s were detected in $CoFe_2O_4/BiVO_4$ (Fig. 6B). The binding peaks at 158 eV and 164 eV were in accordance with Bi $4f_{2/7}$ and $4f_{2/5}$, respectively. The banding peak of $V2p_{3/2}$ was at around 516 eV. The peak at about 529 eV could be attributed to O1 s of the lattice oxide species, while the banding peak at around 530 eV was in correspondence with adsorbed oxygen species on the surface [35,36]. After loading nickel ferrite and cobalt ferrite particles, respectively, the peaks of Ni, Fe and Co can be detected correspondingly. The banding peak of Ni $2p_{3/2}$ arised at about 855 eV. The peaks at 781 eV and 796 eV can be assigned to Co $2p_{3/2}$ and Co $2p_{1/2}$ [12,37]. As previous reports suggested, the peaks at about 710 eV ($2\,p_{3/2}$) and 724 eV ($2\,p_{1/2}$) in Fe 2p XPS spectra is a convincible evidence to confirm the oxidation state of the Fe^{3+} [38]. The peak at 284 eV corresponded to the C1s orbital peak, which may be caused by the contamination of the carbon during the test [36].

The optical properties of all photoelectrodes were assessed by testing UV–vis diffuse reflectance spectrum. As can be seen from Fig. 7, the absorption edge of pure $BiVO_4$ film was located at about 506 nm. Accordingly [39], the absorption edge of photoelectrodes has a red-shift after loading $NiFe_2O_4$ and $CoFe_2O_4$ nanoparticles onto the surface of leaf structure $BiVO_4$ electrodes, which is in favor of efficiently exploiting solar light and generating high photocurrent response. So as to explain interparticle electrons transferring behavior, optical activity of $NiFe_2O_4$ and $CoFe_2O_4$ powder were measured, respectively (Fig. S7). The band gap energy (E_g) of products was estimated to be 2.45 eV, 1.77 eV and 1.70 eV according to the formula ($Eg = \frac{1240}{\lambda}eV$) [24–26,32]. The conduction band (CB) and valence band (VB) position of all semiconductors were caculated using the formula:

$$E_{CB} = \chi - E^{\theta} - \frac{1}{2}E_g; E_{VB} = E_{CB} + E_g$$

χ is electronegativity of the semiconductor, which are 6.04 eV, 4.65 eV and 5.30 eV, respectively. E^{θ} is the energy of free electrons on the hydrogen scale (4.5 eV) [40]. The CB position of $BiVO_4$, $NiFe_2O_4$ and $CoFe_2O_4$ were computed as 0.30 eV, −0.73 eV and −0.05 eV, respectively. The VB positions were afterwards estimated as 2.75 eV, 1.04 eV and 1.65 eV, respectively.

The LSV curves of pure $BiVO_4$, $NiFe_2O_4/BiVO_4$ and $CoFe_2O_4/BiVO_4$ photoanodes are recorded in Fig. 8. The photocurrent density of as-obtained three samples sharply increases with the light on. The photocurrent density of optimal electrode $CoFe_2O_4/BiVO_4$ reach to 0.65 mA cm^{-2} at 1.23 V vs. RHE, which were 1.75 times and 3.25 times increment compared to the planar $BiVO_4$ (0.20 mA cm^{-2}) and $NiFe_2O_4/BiVO_4$ (0.35 mA cm^{-2}) film, respectively. $NiFe_2O_4$ and $CoFe_2O_4$ were deposited onto the surface of $BiVO_4$ to form $NiFe_2O_4/BiVO_4$ and $CoFe_2O_4/BiVO_4$ binary heterojunction, which can enlarge the absorption capacity of $BiVO_4$ to visible light range and benefit the transfer and separation of carriers [24–26]. Fig. 8B showed the electrochemical behavior of all photoelectrodes. Comparing with pure $BiVO_4$ film, the onset potentials of $NiFe_2O_4/BiVO_4$ and $CoFe_2O_4/BiVO_4$ films were 1.405 V and 1.398 V (vs. Ag/AgCl, at J~1.0 mA cm^{-2}), respectively. The negative shifts of onset potential with composites indicated that loading $NiFe_2O_4$ and $CoFe_2O_4$ nanoparticles could reduce the collective holes on the surface of $BiVO_4$, significantly decreasing the combination rate of carriers in the process of water oxidation,

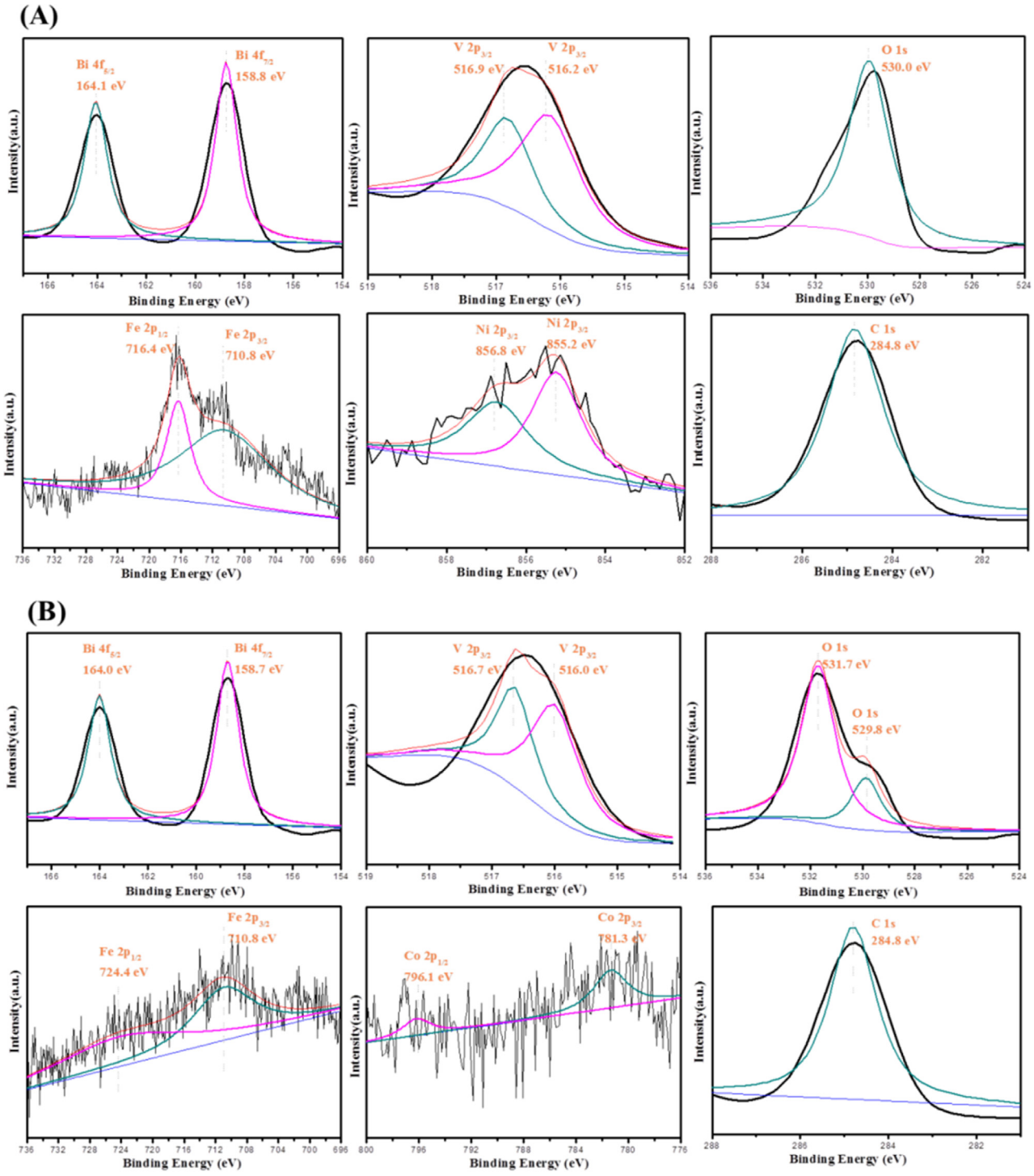

Fig. 6. The XPS survey spectra of Bi, V, O Fe, Ni and Co elements as the main elements.

which is similar to co-catalytic effect of α-Fe_2O_3, Co_3O_4 and NiO [41].

To further study the transport behavior of charge carries and response to light on photoelectrodes, the photocurrent-time curves and IPCE values were recorded in Fig. 9. The light effect on the recombination of carriers was proved through light turning up/off process of the chronoamperometry method when the light was turned off, the glorious photocurrent density of as-obtained electrodes was quenched immediately and eventually tends to 0, owing to the rapid recombination and the poor dark current of $BiVO_4$ and $BiVO_4$ composites [6,15]. Both the IPCE and photocurrent results were in corresponding with LSV analysis. As shown in Fig. 8B, the IPCE value was calculated by the following equation [42]:

$$\mathrm{IPCE}\,(\%) = \frac{(1240 \times \mathrm{J})}{(\lambda \times \mathrm{P})} \times 100\%$$

The *J* is the photocurrent density. λ is the incident wavelength of the monochromatic light. *P* is the power density of light at different wavelength. In the range 350–500 nm, the IPCE value of composites were higher than that of pristine $BiVO_4$. The IPCE values of three

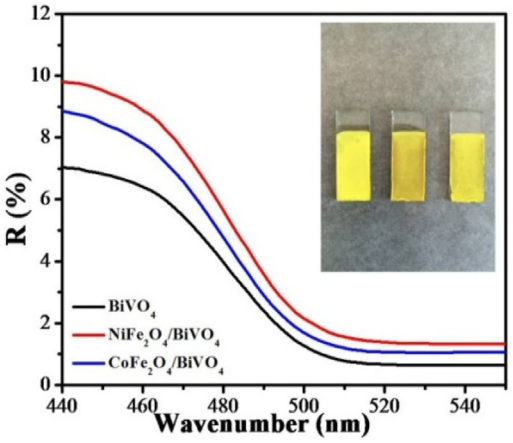

Fig. 7. UV–vis diffuse reflectance spectrum of $BiVO_4$, $NiFe_2O_4/BiVO_4$ and $CoFe_2O_4/BiVO_4$ electrodes, respectively. The insert is digital photo of above the three film.

samples reached to 3.4%, 10.2% and 15.5% at 370 nm, respectively. As the wavelength shifted to 460 nm, the IPCE values were up to 2.0%, 5.0% and 6.7% at, respectively. It confirmed that $NiFe_2O_4$ and $CoFe_2O_4$ nanoparticles can enhance light absorption and reduce the combination of electrons and holes. Magnetic nanoparticles used in the field of photocatalysis the biggest advantage is the effective recovery after the reaction.

Fig. 10 shows MFe_2O_4 (Ni, Co)/$BiVO_4$ composites as photoanodes could acquire more hydrogen under visible light illumination in 3 h rather than that of pure $BiVO_4$ electrode. The three photoelectrodes $BiVO_4$, $NiFe_2O_4/BiVO_4$ and $CoFe_2O_4/BiVO_4$ were capable of generating 209 μmol, 257 μmol, and 476 μmol H_2 in 1 mL of pumped gas in photo-reactor, respectively. And all results of hydrogen evolution were consistent with above measurements of PEC performance, showing the splendid PEC hydrogen production activity of these composites.

Electrochemical impedance spectroscopy (EIS) of the selected samples was assessed to explore transfer properties of charge carries and enhanced PEC performance. And the Nyquist plots were recorded in Fig. 11. The Nyquist plots exhibited all the electrodes

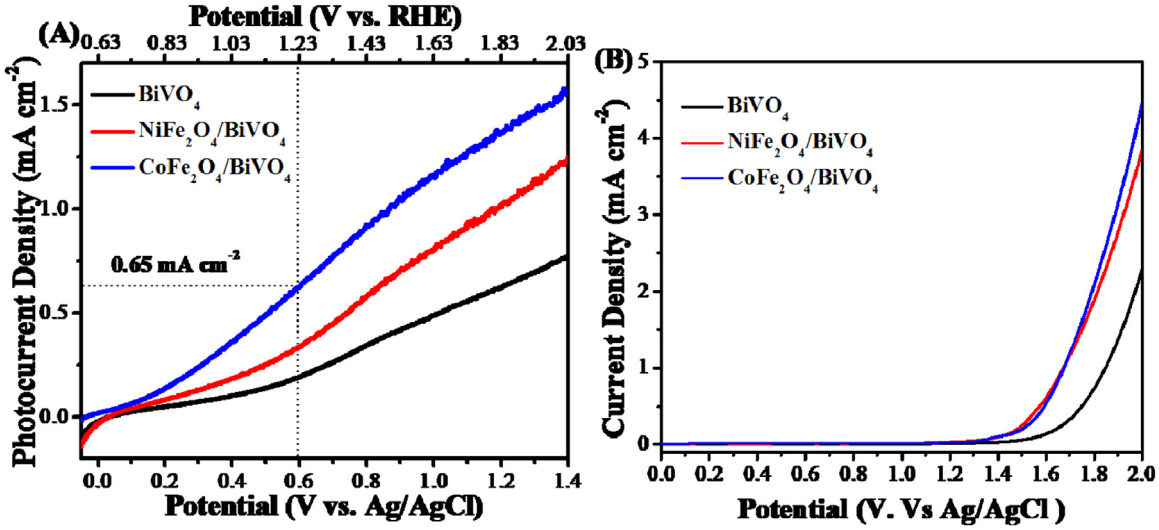

Fig. 8. Linear current-voltage curves with a scan rate of 50 mV s^{-1} of $BiVO_4$, $NiFe_2O_4/BiVO_4$ and $CoFe_2O_4/BiVO_4$ photo-electrodes (A) with illumination and (B) without light irradiation, respectively;.

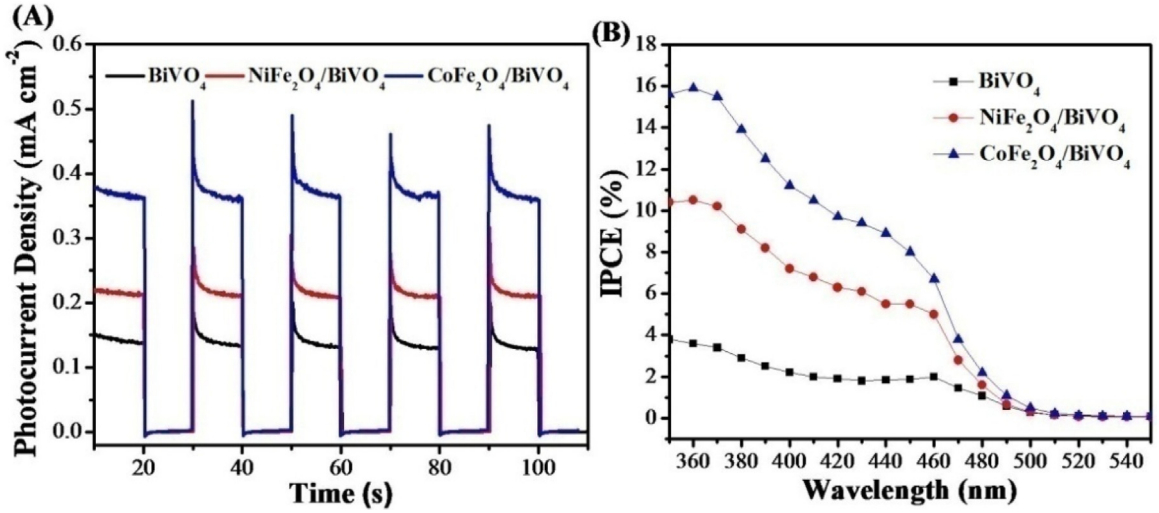

Fig. 9. (A) I-t curves of pure $BiVO_4$, $NiFe_2O_4/BiVO_4$ and $CoFe_2O_4/BiVO_4$ photo-electrodes at 1.23 V vs. REH bias potential in 0.5 M Na_2SO_4 (pH ~ 7.35). (B) IPCE value of pure $BiVO_4$, $NiFe_2O_4/BiVO_4$ and $CoFe_2O_4/BiVO_4$ photo-electrodes at the incident wavelength range from 350 nm–550 nm at 1.23 V vs. NHE bias potential in 0.2 M Na_2SO_4 solution.

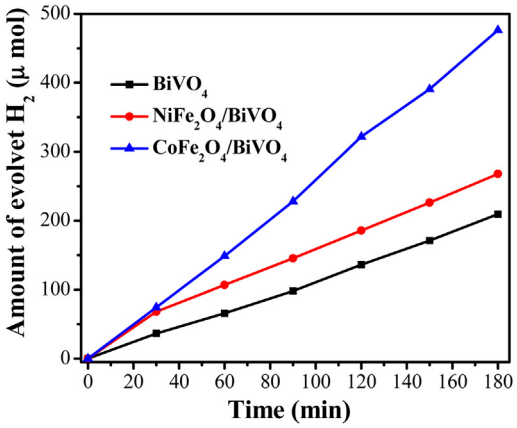

Fig. 10. Time course of produced H_2 at 1.23 V vs. RHE in pure 0.5 M Na_2SO_4 (pH ~ 7.35).

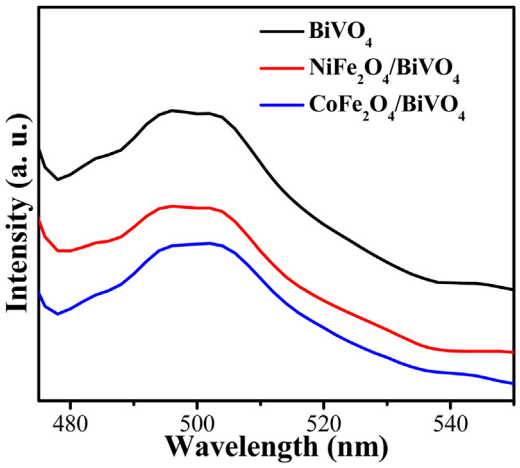

Fig. 12. PL spectra of the as-synthesized samples: $BiVO_4$, $NiFe_2O_4/BiVO_4$ and $CoFe_2O_4/BiVO_4$.

were consistent with LSV and I-t curves with light and without light irradiation. And the semicircle of the $CoFe_2O_4/BiVO_4$ was smaller than either the neat $BiVO_4$ or $NiFe_2O_4/BiVO_4$ composite electrode in both dark and illuminating condition, respectively, indicating the high efficiency of electrons and holes transport in the interface between semiconductor and electrolyte [43].

Photoluminescence technology is an effective approach to study the separation and recombination behaviors of photo-induced electron-hole pairs. Theoretically, the intensity of photoluminescence would indicate the photocatalytic activity to some extent. Fig. 12 is photoluminescence emission spectra of samples at excitation wavelength 350 nm. All films possessed the primary PL peak of predominant $BiVO_4$ at about 506 nm emission wavelength, which was consistent with absorption edge of DRS analysis. And the PL intensities of loaded-style $NiFe_2O_4/BiVO_4$ and $CoFe_2O_4/BiVO_4$ films were lower than that of pure $BiVO_4$ film, showing that electrons and holes of $MFe_2O_4/BiVO_4$ (M = Ni, Co) films could be separated easily. [44–46].

In order to further analyze and propose the possible mechanism of PEC water splitting reaction, Motty-Schottky curves were measured as shown in Fig. 13. $BiVO_4$ is commonly known as n-type semiconductor with a positive slope. Through fitting the linear part of the plots, the flat band potentials were approximately estimated as −0.61 V, −0.51 V and −0.69 V vs. Ag/AgCl, respectively. The lower scopes in Motty-Schottky curves of both $CoFe_2O_4/BiVO_4$

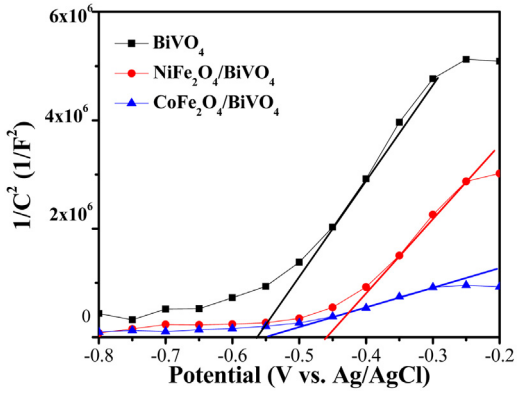

Fig. 13. Mott-Schottky curves of (a) pure $BiVO_4$; (b) $NiFe_2O_4/BiVO_4$; (c) $CoFe_2O_4/BiVO_4$ in the dark 0.2 M Na_2SO_4.

and $NiFe_2O_4/BiVO_4$ photoelectrodes as compared to the pure $BiVO_4$ electrode suggested the greatly enhanced donor densities. The

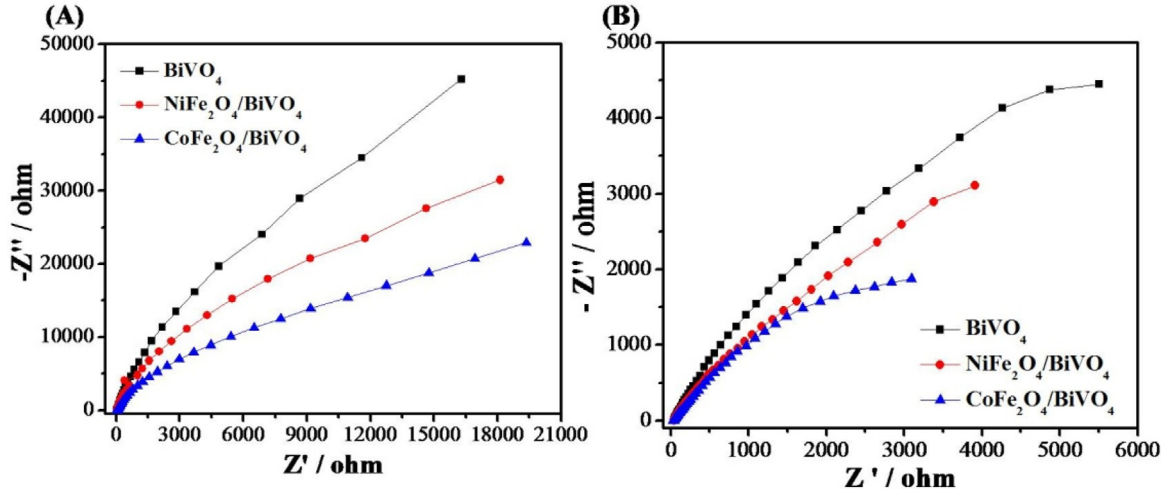

Fig. 11. Nyquist plots of EIS measurements on the pure $BiVO_4$, $NiFe_2O_4/BiVO_4$ and $CoFe_2O_4/BiVO_4$ electrodes (A) in the dark at the open circuit potential; (B) under the visible light irradiation at the open circuit potential in 0.5 M Na_2SO_4 (pH ~ 7.35).

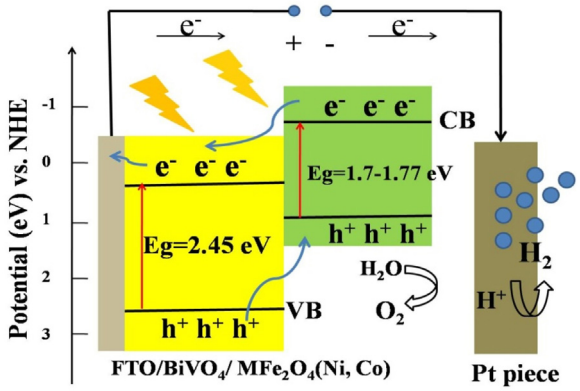

Fig. 14. The possible PEC hydrogen generation mechanism of MFe_2O_4 (M = Ni, Co)/$BiVO_4$ electrodes at 1.23 V vs. REH in 0.5 M Na_2SO_4 under visible light.

donor density (N_d) can be calculated according to the following equation [9]:

$$\frac{1}{C^2} = \frac{2}{e_0 \varepsilon \varepsilon_0 A^2 N_d}\left[(V - V_{FB}) - \frac{KT}{e_0}\right]$$

C is the depletion layer capacitance, e_0 is the electron charge, ε is the dielectric constant (~86), ε_0 is the permittivity of vacuum, V_{FB} is flat band potential, V is electrode applied potential and A is electrode area. The calculated results of carried density (N_d) reach 2.7×10^{17} cm^{-3},4.4×10^{17} cm^{-3},1.5×10^{18} cm^{-3}, respectively, demonstrating the carriers density of $BiVO_4$ electrodes were increased by surface modification of $NiFe_2O_4$ and $CoFe_2O_4$ magnetic nanoparticles, and with a superior PEC hydrogen activity due to the effective separation and transfer of charge carriers at the interface of photoelectrode and conductive substrate [47].

Basing on the results of DRS and PEC measurements, the possible mechanisms of PEC water splitting reaction are proposed and presented in Fig. 14. The CB and VB positions of individual semiconductor have been estimated by DRS data, respectively. During phtocatalytic reaction, the electrons appeared in the VB of catalysts, while the same amount of holes were generated in CB as the semiconductors were excited by high-energy light. The electrons in the CB of $NiFe_2O_4$ or $CoFe_2O_4$ transferred to CB of $BiVO_4$ because the CB edge position of MFe_2O_4 (M = Ni, Co) is more negative than that of $BiVO_4$. On the other hand, the holes in VB of $BiVO_4$ transferred to the VB of MFe_2O_4 (M = Ni, Co) and consequently resulted in the enhanced PEC activities [48]. The electron in transferred from photocatalysts to FTO substance in order before it reached to Pt electrode through external circuit. Finally generating hydrogen via reduction reaction of water. In brief, four main influences were proposed for PEC reaction. Primarily, the leaf-like structure new $BiVO_4$ film is acquired; Second, the construction of energy-matched n-n and *p-n* junctions are beneficial to the separation of electron-hole pairs as well as PEC activity. Besides, $BiVO_4$ photoanode has stronge capacity of absorption of sunlight after combination with $NiFe_2O_4$ or $CoFe_2O_4$ nanoparticles, owing to the improved photocurrent response of $BiVO_4$. Finally, enhancement of the carries density in $BiVO_4$ electrodes would lead to an enhanced PEC performance.

4. Conclusion

In this work, a new leaf-like structure $BiVO_4$ was prepared in high concentration electrolyte with addition of Zn^{2+} as structure-directing agent. Magnetic $NiFe_2O_4$ and $CoFe_2O_4$ nanoparticles were successfully loading on the surface of $BiVO_4$ to construct n-n and *p-n* heterojunction via electrophoretic deposition process. Formation of these heterojunctions can effectively prevent carriers from recombining and accelerate the separation of electrons and holes. Hence, the photocurrent density of $NiFe_2O_4/BiVO_4$ and $CoFe_2O_4/BiVO_4$ are higher than of pure $BiVO_4$ electrode at 1.23 V vs NHE, which indicates the composites possess excellent PEC activity. And the result of hydrogen evolution demonstrates these new photoanodes exhibiting superior hydrogen generation performance.

Acknowledgements

This work was financially supported by the National Natural Science Foundation of China (21663027, 51262028, 21261021), the Science and Technology Support Project of Gansu Province (1504GKCA027), the Program for the Young Innovative Talents of Longyuan, the Program for Innovative Research Team(NWNU-LKQN-15-2) and the Undergraduate Academic Innovative Research Team of Northwest Normal University.

Appendix A. Supplementary data

Supplementary data associated with this article can be found, in the online version, at http://dx.doi.org/10.1016/j.apcatb.2017.05.044.

References

[1] J.C. Bian, C. Huang, L.Y. Wang, T.F. Hung, W.A. Daoud, R.Q. Zhang, ACS Appl. Mater. Interfaces 6 (2014) 4883–4890.
[2] C.J. Liu, Y.H. Yang, W.Z. Li, J. Li, Y.M. Li, Q.L. Shi, Q.Y. Chen, ACS Appl. Mater. Interfaces 7 (2015) 10763–10770.
[3] S.K. Mohapatra, S. Banerjee, M. Misra, Nanotechnology 19 (2008) 315601.
[4] K. Sayama, A. Nomura, T. Arai, T. Sugita, R. Abe, M. Yanagida, T. Oi, Y. Iwasaki, Y. Abe, H. Sugihara, J. Phys. Chem. B 110 (2006) 11352–11360.
[5] Y.H. Ng, A. Iwase, A. Kudo, R. Amal, J. Phys. Chem. Lett. 1 (2010) 2607–2612.
[6] L.W. Zhang, E. Reisner, J.J. Baumberg, Energy Environ. Sci. 7 (2014) 1402–1408.
[7] S.P. Berglund, D.W. Flaherty, N.T. Hahn, A.J. Bard, C.B. Mullins, J. Phys. Chem. C 115 (2011) 3794–3802.
[8] K. Sayama, A. Nomura, Z.G. Zou, R. Abe, Y. Abeb, H. Arakawa, Chem. Commun. (2003) 2908–2909.
[9] J. Resasco, H. Zhang, N. Kornienko, N. Becknell, H. Lee, J.H. Guo, A.L. Briseno, P.D. Yang, ACS Cent. Sci. 2 (2016) 80–88.
[10] T.W. Kim, K.S. Choi, Science 990 (2014) 343.
[11] L.G. Xia, J. Bai, J.H. Li, Q.Y. Zeng, X.J. Li, B.X. Zhou, Appl. Catal. B: Environ. 183 (2016) 224–230.
[12] M. Zhong, T. Hisatomi, Y.B. Kuang, J. Zhao, M. Liu, A. Iwase, Q.X. Jia, H. Nishiyama, T. Minegishi, M. Nakabayashi, N. Shibata, R. Niishiro, C. Katayama, H. Shibano, M. Katayama, A. Kudo, T. Yamada, K. Domen, J. Am. Chem. Soc. 137 (2015) 5035–5060.
[13] B. Zhou, J.H. Qu, X. Zhao, H.J. Liu, J. Environ. Sci. 23 (2011) 151–159.
[14] A. Iwase, A. Kudo, J. Mater. Chem. 20 (2010) 7536–7542.
[15] W.J. Luo, Z.S. Yang, Z.S. Li, J.Y. Zhang, J.G. Liu, Z.Y. Zhao, Z.Q. Wang, S.C. Yan, T. Yu, Z.G. Zou, Energy Environ. Sci. 4 (2011) 4046–4051.
[16] M.L. Sebastián, F. Cristian, M.S. Damián, D.H.A. María, P.P. Germán, M. Alex, R.M. Juan, A. Teresa, ACS Appl. Mater. Interfaces 8 (2016) 4076–4085.
[17] Y. Zhang, D. Wang, X.T. Zhang, Y. Chen, L.N. Kong, P. Chen, Y.L. Wang, C.H. Wang, L.L. Wang, Y.C. Liu, Electrochim. Acta 195 (2016) 51–58.
[18] T.W. Kim, K.S. Choi, J. Phys. Chem. Lett. 7 (2016) 447–451.
[19] K.H. Ye, Z.S. Chai, J.W. Gu, X. Yu, C.X. Zhao, Y.M. Zhang, W.J. Mai, J. Nano Energy Power Res. 18 (2015) 222–231.
[20] D. Kang, Y. Park, J.C. Hill, K.S. Choi, J. Phys. Chem. Lett. 5 (2014) 2994–2999.
[21] H.R. Kima, G. Kimb, S.I. Ina, Y. Parkb, Electrochim. Acta 189 (2016) 252–258.
[22] F. Ding, W. Xu, G.L. Graff, J. Zhang, M.L. Sushko, X.L. Chen, Y.Y. Shao, M.H. Engelhard, Z.M. Nie, J. Xiao, X.J. Liu, P.V. Sushko, J. Liu, J.G. Zhang, J. Am. Chem. Soc. 135 (2013) 4450–4456.
[23] W.H. He, R.R. Wang, C. Zhou, J.J. Yang, F. Li, X. Xiang, Ind. Eng. Chem. Res. 54 (2015) 10723–10730.
[24] E.S. Kim, H.J. Kang, G. Magesh, J.Y. Kim, J.W. Jang, J.S. Lee, ACS Appl. Mater. Interfaces 6 (2014) 17762–17769.
[25] H. Jung, S.Y. Chae, C. Shin, B.K. Min, O.S. Joo, Y.J. Hwang, ACS Appl. Mater. Interfaces 7 (2015) 5788–5796.
[26] L. Yan, W. Zhao, Z.F. Liu, Dalton Trans. 45 (2016) 11346–11352.
[27] Y.Q. Shi, K.Q. Zhou, B.B. Wang, S.H. Jiang, X.D. Qian, Z. Gui, R.K.K. Yuen, Y. Hu, J. Mater. Chem. A 2 (2014) 535–544.
[28] J. Zeng, T. Song, M.X. Lv, T.T. Wang, J.Y. Qin, H.P. Zeng, RSC Adv. 6 (2016) 54964–54975.
[29] G.Y. He, J.J. Ding, J.G. Zhang, Q.L. Hao, H.Q. Chen, Ind. Eng. Chem. Res. 54 (2015) 2862–2867.

[30] S. Duangjama, K. Wetchakun, S. Phanichphant, N. Wetchakun, Mater. Lett. 181 (2016) 86–91.
[31] M. Sui, C. Han, Y. Wang, J.J. Li, X.Q. Gu, J. Mater. Sci.: Mater. Electron. 27 (2016) 4290–4296.
[32] Y.Y. Luo, G.Q. Tan, G.H. Dong, L.L. Zhang, J. Huang, W. Yang, C.C. Zhao, H.J. Ren, Appl. Surf Sci. 324 (2015) 505–511.
[33] M.R.D. Silva, A.C. Lucilha, R. Afonso, L.H. Dall'Antonia, L.V.D.A. Scalvi, Ionics 20 (2014) 105–113.
[34] Z.B. Jiao, T. Chen, H.C. Yu, T. Wang, G.X. Lu, Y.P. Bi, J. Colloid Interface Sci. (2014) 41995–42101.
[35] Y. Zhang, D. Wang, X.T. Zhang, Y. Chen, L. Kong, P. Chen, Y.L. Wang, C.H. Wang, L.L. Wang, Y.C. Liu, Electrochim. Acta 195 (2016) 51–58.
[36] M.C. Biesingera, B.P. Paynec, A.P. Grosvenord, L.W.M. Laua, A.R. Gersonb, R.S.C. Smartb, Appl. Surf. Sci. 257 (2011) 2717–2730.
[37] J. Xu, W.Z. Wang, J. Wang, Y.J. Jiang, Appl. Surf. Sci. 349 (2015) 529–537.
[38] Y.D. Ma, X.P. Dai, M.Z. Liu, J.X. Yong, H.Y. Qiao, X. Jin, Z.Z. Li, X.L. Huang, H. Wang, X. Zhang, ACS Appl. Mater. Interfaces 8 (2016) 34396–34404.
[39] Y. Ma, Y.L. Jia, L.N. Wang, M. Yang, Y.P. Bi, Y.X. Qi, Phys. Chem. Chem. Phys. 18 (2016) 5091–5094.
[40] X. Lin, X.Y. Guo, W.L. Shi, L.N. Zhao, Y.S. Yan, Q.W. Wang, J. Alloys Compd. 635 (2015) 256–264.
[41] L.G. Xia, J. Bai, J.H. Li, Q.Y. Zeng, L.S. Li, B.X. Zhou, Appl. Catal. B 204 (2017) 127–133.
[42] J.Y. Gan, X.H. Lu, B.B. Rajeeva, R. Menz, Y.X. Tong, Y.B. Zheng, ChemElectroChem 2 (2015) 1385–1395.
[43] S.L. Xie, T. Zhai, Y.J. Zhu, W. Li, R.L. Qiu, Y.X. Tong, X.H. Lu, Int J. Hydrogen Energy 39 (2014) 4820–4827.
[44] M. Wang, P.Y. Guo, T.Y. Chai, Y.H. Xie, J. Han, M.Y. You, Y.Z. Wang, Z. Tong, J. Alloys Compd. 691 (2017) 8–14.
[45] X. Lin, D. X, J., Zheng, M. S. Song, G. B. Che, Y. S. Wang, Y., Yang, C., Liu, L. N. Zhao and L. M. Chang, J. Alloys Compd. 688 (2016) 891–898.
[46] Y.Q. Zhai, Y.J. Yin, X. Liu, Y.M. Li, J.Y. Wang, C.C. Liu, G. Bian, Mater. Res. Bull. 89 (2017) 297–306.
[47] C.J. Liu, Y.H. Yang, W.Z. Li, J. Li, Y.M. Li, Q.L. Shi, Q.Y. Chen, ACS Appl. Mater. Interfaces 7 (2015) 10763–10770.
[48] N. Wetchakun, S. Chaiwichain, B. Inceesungvorn, K. Pingmuang, S. Phanichphant, A.I. Minett, J. Chen, ACS Appl. Mater. Interfaces 4 (2012) 3718–3723.